Behavior of microbubbles on spatially controlled golden nanoparticles

Xiumei Liu (刘秀梅) and Mingli Jiao (焦明礼)*

School of Mechatronic Engineering, China University of Mining and Technology, Xuzhou 221116, China
**Corresponding author: liuxmcumt@126.com*

Received April 19, 2016; accepted June 14, 2016; posted online July 14, 2016

Incipient plasmonic bubble formation is observed around gold nanopillars with different inter-nanopillar separations. The experimental measurements and theoretical analysis show that the nanobubble formation is due to the enhanced plasmonic resonance rather than from the laser heating. Inter-nanopillar distribution may lead to threshold fluence variations. The lifetime of plasmonic bubbles can reach several minutes. Furthermore, both the radius and the growth rate of the plasmonic nanobubble increase as the inter-nanopillar distribution decreases. Smaller-spacing distributed arrays produced larger bubbles. The maximum growth rate of the bubbles can be reached at about 883.5×10^{-6} m/s on 1 μm nanopillars, but it is only 56.9×10^{-6} m/s on 4 μm nanopillars.

OCIS codes: 140.3390, 000.2190, 060.3510, 140.3535.
doi: 10.3788/COL201614.081402.

The increasing interest in golden nanoparticles nowadays is coming from the fundamentally new properties that they express and that have related to them opportunities for new applications[1,2]. The generation of nanobubbles around plasmonic nanostructures opened new trends, especially in biology and medicine, including in photothermal cancer therapy[3], photothermal imaging[4], drug and gene delivery[5], and photoacoustic imaging[6]. For example, in terms of imaging, there has been widespread interest in using plasmonic nanoparticles as contrast agents for photoacoustic imaging. For therapeutic applications, nanoparticle-targeted regions of tissue can be selectively heated using continuous wave (CW) laser sources, producing hyperthermia and inducing cell death in the targeted region[7,8]. To gain detailed insight into the physical mechanisms of these applications and resultantly improve the efficiency, it is important to quantitatively understand the physical behavior of individual nanobubbles[9].

When a CW laser with a wavelength coinciding with the plasmon resonance of the golden nanoparticles is focused onto the substrate, it resonantly excites the electronic plasmon modes in the nanostructure, and this energy is converted to lattice vibrations on a picosecond time scale. This results in very rapid heating of the golden particle, and this heat is quickly transferred to the surrounding fluid, causing it to be vaporized and the bubble to grow[10]. This generated plasmonic bubble grows continually for tens of minutes without collapsing. The most promising direction of nanoparticle applications, however, is combining the photothermal properties of plasmonic (gold) nanoparticles with the mechanical and optical properties of transient plasmonic nanobubbles in a variety of medical applications, including nanoparticle-based imaging, diagnostics, and therapies, including drug delivery with gold nanoparticles[11–14] and, ultimately, for theranostics[10,15].

Numerous studies have been conducted over the past 50 years to understand the formation of photothermal bubble generation mainly under pulsed illumination[16]. In fact, the plasmonic bubble generation under CW illumination had received considerable attention until recently[17]. In 2009, Adleman *et al.*[18] were the first scholars who focused a CW laser on a flowing ethanol-water mixture over gold nanoparticles and provided the necessary heat of heterogeneous catalysis. In 2012, Hühn *et al.*[19] studied bubble generation around nanoparticles under CW heating and to hypothesize superheating. Zheng *et al.*[20] investigated a vapor bubble created by a focused CW laser beam on the surface of a silver film and changed the diameter and velocity of the vapor bubble by tuning the laser power. In 2013, Oara *et al.*[21] described the bubble generation around metal nanoparticles under illumination theoretically, based on simple thermodynamics considerations. Zhao *et al.*[22] proposed a first application of plasmon-induced microbubbles (MBs) that consisted of generating a surface MB on a metal film as an effective lens for surface plasmon waves in a microfluidic environment. In 2014, Baffou *et al.*[17] investigated a temperature threshold for plasmonic bubble formation, explained their unexpectedly long lifetime, and described the MB steady state maintained under CW illumination. Lombard *et al.*[23] addressed the kinetics of formation of the nanobubbles using a hydrodynamic free-energy model. They proved that the expansion of nanobubble radius is adiabatic and the collapse is an isothermal evolution. Hou *et al.*[24] investigated the explosive formation and dynamics of vapor nanobubbles around a continuously heated gold nanosphere. However, despite these few recent breakthroughs in plasmonics, the mechanisms involved in plasmonic bubble formation are far from being understood, and the potential application are not exhaustively described. In this Letter, the nature of the plasmonic bubble generation is presented. The expansion and shrinkage of plasmonic bubbles created by different inter-golden nanopillars heated under CW laser illumination is described,

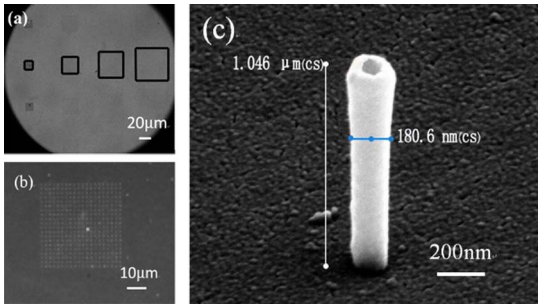

Fig. 1. (a) Optical images of the gold nanopillar arrays. (b) Optical image of the gold nanopillar array with the spacing of 1 μm. (c) Scanning electron microscope image of an individual gold nanopillar.

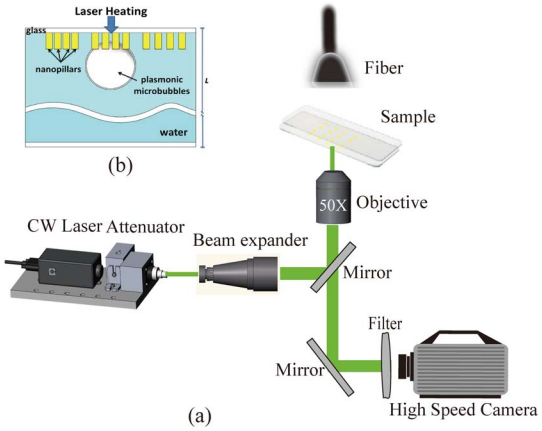

Fig. 2. Schematic of the experimental setup.

and the effect of spatial control on the diameter and the expanding velocity of plasmonic bubbles is also explained.

The substrate consists of a uniform array of vertical gold nanopillars on a quartz coverslip. There is a matrix of 4×4 quadrants of vertical nanotubes made of gold fabricated on the substrate, with the inter-nanopillars varying from 1 to 4 μm (Fig. 1(a)), which increases with the columns on the substrate. Each quadrant contains 20×20 gold nanopillars (Fig. 1(b)), and these three-dimensional nanopillars have a hollow nanostructure (Fig. 1(c)). The nanopillars consist of a polymeric hollow nanocylinder with internal and external diameters of, respectively, 100 and 130 nm. On the external nanocylinder wall, a 25 nm-thick gold layer is deposited, resulting in a total external diameter of about 180 nm[25]. The nanocylinders are produced, starting with the polymer spin coated on the quartz coverslip. The final height of the nanocylinders is defined by the thickness of this polymer film and is therefore very homogeneous among the nanostructures. The thickness can be tuned precisely by changing the spinning conditions. For inter-nanopillar of 1 μm, the quadrant will be 19 μm × 19 μm, and the distance between each quadrant is 500 μm.

One advantage of such a sample is that the nanopillar distribution is regular and perfectly uniform in every quadrant. This way, for a given laser beam diameter and power, the plasmonic bubble is the same irrespective of the location of the laser beam on the sample. Besides the uniformity of the nanopillar distribution, the other advantage is the adjustable inter-nanopillar distance. When the laser illuminates different spatially controlled nanopillars on the same sample, such as from 1 to 4 μm, the effect of the inter-nanopillars on the plasmonic bubble can be investigated.

The experimental setup is shown in Fig. 2. A CW laser (Cobolt Samba™) with a 532 nm wavelength is used; its power is controlled by a variable attenuator (Zaber technologies T-RS60A). The laser beam passes through a beam expander (10×) and is then focused on the gold nanopillars from the bottom through the microscope objective (Olympus 50×, 0.45 NA). A filter was used to block the reflected laser light to prevent damage to the camera. The motion of the plasmonic bubble was recorded by a high-speed camera with a frame rate of 500 fps (Photron Fastcam SA2). Illumination for the camera was provided by a fiber lamp (Olympus ILP-1) emitting a light spectrum, part of which passed through the filter to the camera.

To investigate the mechanisms underlying the bubble formation, we produced bubbles with an initial degassing treatment. Here, the Milli-Q water was initially degassed using a sealed round flask connected to an external pump. The water was stirred as the flask was pumped by the vacuum, and the degassing process was complete after one hour, when no more bubbles were visible. The treated water was used in the experiment immediately. Strictly speaking, the degassed water was turned into partially degassed water during the experiments because it was unavoidable that some air re-dissolved in the water.

A drop of degassed water was deposited on top of the sample and then covered with another coverslip to obtain a 1 mm-thick water layer. In such a configuration, the plasmonic resonance of the nanoparticle assembly is located around 532 nm. When such a system is locally illuminated by the CW laser (532 nm), the gold nanopillars are quickly heated up, and as a result, a plasmonic bubble forms around the laser spot on the gold nanopillars. The location and diameter of the plasmonic bubble can be modulated by moving the laser spot on different spatially controlled nanopillars and adjusting the laser power, respectively. It should be noted that, after its generation, the bubble remains in contact with the gold nanopillars, and the lifetime of the plasmonic bubbles can reach several minutes.

The evolution of a bubble produced by a CW laser heated on 1 μm inter-nanopillars of a hydrophilic surface is shown as a series of images in Fig. 3. Initially, the plasmonic bubble appeared rapidly at the top of the 1 μm nanopillars after the degassed water has absorbed 12.97 mW from the laser. The bubble is a small sphere and keeps expanding spherically while the laser is on. It grows slowly for several seconds (Fig. 3(a)–3(h)) and reached its maximum radius at 2.004 s. Then, the bubble

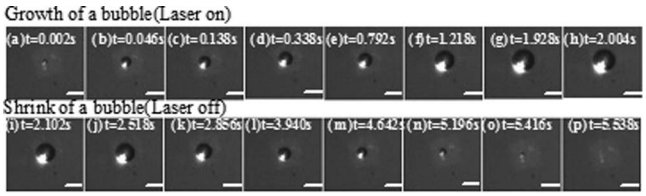

Fig. 3. Sequential images (a)–(h) demonstrate the formation and (i)–(p) show the shrink of a single plasmonic bubble (bottom view) on 1 μm nanopillars. The fluid is degassed water and the absorbed laser power is 12.97 mw.

begins to shrink when the laser is turned off (Fig. 3(h)) and becomes smaller as time goes on (Fig. 3(i)–3(o)). Finally, the bubble is gone at 5.538 s (Fig. 3(p)).

The time evolution of the plasmonic bubble can be obtained by tracking the contour of the bubble, which is shown in Fig. 4. Initially, a bubble is created with an initial diameter of 2.32 μm because the plasmonic resonance is relatively strong. After its creation, the bubble expands for 2.032 s, with the incident laser power being maintained at 12.97 mW, and reaches the maximum radius of bubble (Rmax) 9.22 μm, shown in Phase I of Fig. 4. The bubble exhibits rapid expansion at the beginning of Phase I, but the expansion slows down at the end of this phase. Phase II in Fig. 4 shows that the laser was turned off to induce the shrinkage of the bubbles. The bubbles created in the degassed water promptly shrank after the interruption of the laser because the decrease in temperature returns the water vapor to the liquid. The bubble contracts rapidly at the beginning and undergoes a relatively smooth contraction process before it eventually collapses and disappears. The collapse time is 3.496 s, which is longer than the expansion time. Remarkably, the dynamics of the nanobubbles is asymmetrical: the growth is faster than the collapse. The fact that the plasmonic bubble does not collapse as soon as the heating beam switched off vanishes from the nature of the bubble: it is not made of steam, but of air molecules. If the plasmonic bubbles were made of steam, they would disappear as soon as the heating stopped[17]. Furthermore, the shape of a collapsing bubble is not regular due to the existence of nanopillars, so there are peaks in the picture.

As the three-dimensional plasmonic nanopillars used in our experiment are tunable in space, the effect of spatially controlled nanopillars on the plasmonic bubble could be investigated. The generation of a plasmonic bubble around the golden nanopillars requires a specific threshold of the fluence of the laser power. When the threshold is exceeded, the optical energy is converted to the golden nanopillars by the mechanism of plasmon resonance into a sufficient amount of thermal energy that is rapidly evaporates this nano-environment and provides for the expansion of the nanobubble. Figure 5 shows the threshold for bubble creation on the spatially controlled nanopillars. It is noted that different inter-nanopillars need different laser powers. The experiments were repeated four times. The minimum power needed for the 1 μm nanopillars is 12.97 mW, and 15.18 mW for the 2 μm nanopillars, while it remains at 17.56 mW for the other controlled spatial nanopillars. They are approximately 17%, 35.4%, and 35.4% higher than on the 1 μm nanopillars. The clustering of the plasmonic nanopillars was shown to reduce the plasmonic bubble generation threshold[10].

Below, we provide a quantitative analysis of the correlation between the bubble size and the spatially controlled nanopillars. In order to better study the expansion of the MBs localized on the golden nanoparticles, the incident light power needs to be increased to 17.56 mW. At time $t = 100$ ms, the images of a forming MB on different spatially controlled nanopillars are shown in Fig. 6(a). A noticeable feature is that the bubble size is different with the spatially controlled nanopillars for a given illumination duration. With the increasing nanopillar intensity, the radii of the nanobubbles increase because of the increasing number of excited nanopillars under illumination. Smaller spacing or more densely distributed arrays produced larger bubbles. The number of excited nanopillars is calculated from the nanopillar spacing and from the laser diameter of 2.9 μm, assuming that those pillars outside

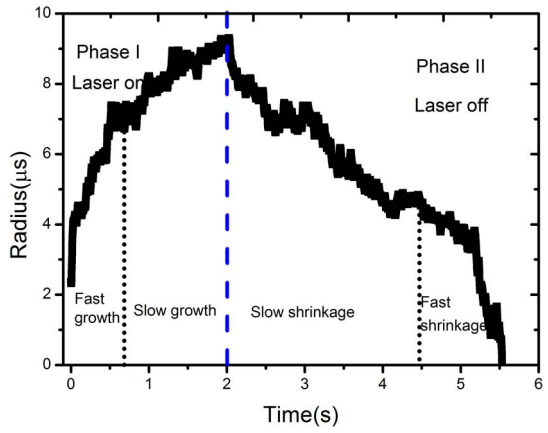

Fig. 4. Plot of the bubble radius versus the time extracted from the top-view images in Fig. 3.

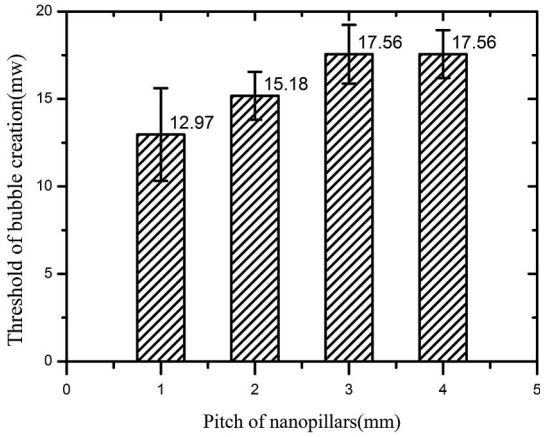

Fig. 5. Threshold of laser power required for the onset of the plasmonic bubble formation in partially degassed water.

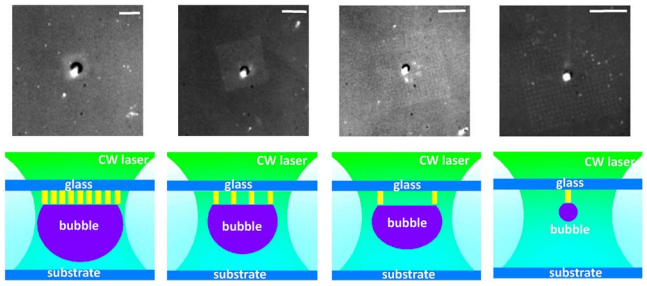

Fig. 6. MB on spatially controlled nanopillars. (a) The images of an MB on different spatially controlled nanopillars at $t = 100$ ms (the error bar is 10 μm). (b) Schematics depicting MB formation due to plasmonic resonance.

of the bubble footprint did not contribute to the heat generation. Within the circular area of illumination, there were 9 pillars for the 1 μm array, 4 pillars for the 2 μm array, 2 pillars for the 3 μm array, and 1 pillar for the 4 μm array, all of which are shown in Fig. 6(b). We also know from the experiments that the bubble on the 4 μm array is produced by heating a single pillar, as the laser had to be aligned to certain locations before the bubble generation. High-density arrays of nanopillars have more power to transform into bubbles by plasmonic resonance.

In the stationary state, the heat and mass generated by the nanopillars reached an equilibrated state with the heat loss to the environment. The heat required to maintain a large bubble is larger than a small bubble, due to the fact that the generated heat from the nanopillars is balanced by the energy loss from the bubble to the surrounding liquid at room temperature. According to Fourier's law, the heat flux out of a spherical bubble with a radius of R and temperature gradient $(\partial_r T)$ at the edge is

$$dQ/dt \approx 4\pi k R \Delta T, \tag{1}$$

where Q is the heat power (J), k is the thermal conductivity of the material $(\mathrm{J\,s^{-1}\,m^{-1}\,K^{-1}})$, and ΔT is the temperature difference across the bubble's surface (K). The temperature difference (ΔT) is assumed to be the same for all the bubbles, so at the steady state, the heat loss from the bubble is proportional to the bubble radius (R).

For the spatially controlled nanopillars varying from 1 to 4 μm, the evolution curves of the bubble in Fig. 6 are obtained and are presented in Fig. 7. The radii of the bubbles are found to increase as the interaction time and the inter-distance of the nanopillars decrease. It indicates that the maximum radius of the bubbles increases as the inter-nanopillars decrease when the laser power is the same. The maximum radii of the bubbles can reach 7.23, 4.47, 3.48, and 1.61 μm for the inter-nanopillars of 1, 2, 3, and 4 μm at 0.3 s, respectively. Clearly, the smaller the inter-nanopillars, the larger the bubbles. This effect can be attributed to nanopillars' density in the case of bubble creation, with high-density arrays of nanopillars absorbing more laser power and thus having more power to transform into bubbles by plasmonic resonance.

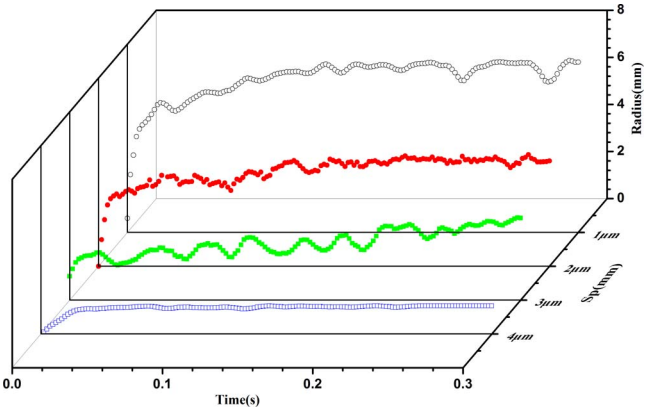

Fig. 7. Plasmonic bubble on different spatially controlled nanopillars in degassed water.

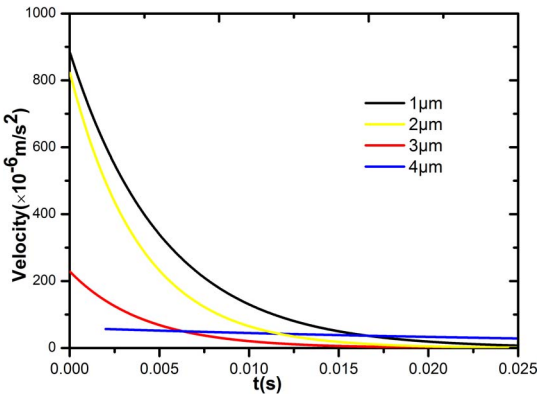

Fig. 8. Bubble growth velocity vs. time on different nanopillars.

Because plasmonic resonance is a rapid process that happens on a picosecond time scale[18], we focus the rapid expansion process of plasmonic bubbles within 0.025 s. Notice that the velocity of the plasmonic bubbles also depends on the inter-nanopillars. By simulating the radius curve, the velocity of the bubbles can be derived by differentiating the simulated curve, as shown in Fig. 8. It is shown that at the moment the laser heats the nanopillars, the growth rate of the bubbles is as high as 883.5×10^{-6} m/s. The velocity of the bubble on the 1 μm inter-nanopillar decreases exponentially from 883.5×10^{-6} to 7.4×10^{-6} m/s within 0.025 s. Furthermore, the initial bubble growth rates on different inter-nanopillars are obviously not the same. The maximum growth velocity of the bubbles on the 1 μm nanopillar is 883.5×10^{-6} m/s, and reaches 822.6×10^{-6} m/s on the 2 μm nanopillars and 225.4×10^{-6} m/s on the 3 μm nanopillars, while it reaches just 56.9×10^{-6} m/s on the 4 μm nanopillars. The larger the inter-nanopillar is, the smaller the growth velocity is.

In conclusion, a detailed experimental study is performed on plasmonic bubbles generated by exposing different spatially controlled nanopillars to CW laser power. With the help of golden nanopillars, the plasmonic resonance is enhanced, and bubbles are efficiently created.

The results demonstrate the significant impact of spatially controlled golden nanopillars on the nucleation and amplification of the cavitation process. In the case of the expanding bubble, the inter-nanopillar distribution may lead to threshold fluence variations. The maximum radius of the plasmonic bubbles decreases as the inter-nanopillars increase because of the high-density arrays of nanopillars absorbing and having more power to transform into bubbles by plasmonic resonance. Furthermore, the initial bubble growth rates on different spatially controlled golden nanopillars are obviously different. The larger the inter-nanopillar is, the smaller the growth velocity is. These effects can be achieved at well below the maximum permissible exposure (MPE) for tissues and the mechanical index (MI) limit for diagnostic ultrasounds, making the approach attractive for both inducing and monitoring nanoparticle-mediated tissue therapy.

The authors thank Xuehua Zhang for the advice, discussions, and support and Detlef Lohse, Chao Sun, and Sander Wildeman for providing technical assistance. This work was supported by the Fundamental Research Funds for the Central Universities (No. 2014QNA39), the Outstanding Young and Middle-Aged University Teachers and Presidents Training Abroad Project of Jiangsu Province, and the Priority Academic Program Development of Jiangsu Higher Education Institutions (PAPD).

REFERENCES

1. A. Polman, ACS Nano **7**, 15 (2013).
2. S. M. Hamidi and M. A. Oskuei, Chin. Opt. Lett. **12**, 031601 (2014).
3. S. Lal, S. E. Clare, and N. J. Halas, Acc. Chem. Res. **41**, 1842 (2008).
4. L. Cognet, S. Berciaud, D. Lasne, and B. Lounis, Anal. Chem. **80**, 2288 (2008).
5. M. Delcea, N. Sternberg, A. M. Yashchenok, R. Georgieva, H. Baeumler, H. Moehwald, and A. G. Skirtach, ACS Nano **6**, 4169 (2012).
6. C. Kim, E. C. Cho, J. Chen, K. H. Song, L. Au, C. Favazza, Q. Zhang, C. M. Cobley, F. Gao, Y. Xia, and L. V. Wang, ACS Nano **4**, 4559 (2010).
7. X. Yang, E. W. Stein, S. Ashkenazi, and L. V. Wang, Wiley Interdiscip Rev. Nanomed. Nanobiotechnol. **1**, 360 (2009).
8. S. Y. Emelianov, P.-C. Li, and M. O'Donnell, Phys. Today **62**, 34 (2009).
9. X. Huang, P. K. Jain, I. H. El-Sayed, and M. A. El-Sayed, Lasers Med. Sci. **23**, 217 (2008).
10. E. Y. Lukianovahleb, A. O. Oginsky, A. P. Samaniego, D. L. Shenefelt, D. S. Wagner, J. H. Hafner, M. C. Farachcarson, and D. O. Lapotko, Theranostics **1**, 3 (2011).
11. D. Lapotko, Nanomedicine **4**, 813 (2009).
12. L. Tong, Q. Wei, A. Wei, and J. X. Cheng, Photochem. Photobiol. **85**, 21 (2009).
13. C. R. Patra, R. Bhattacharya, D. Mukhopadhyay, and P. Mukherjee, Adv. Drug Delivery Rev. **62**, 346 (2010).
14. N. L. Rosi, D. A. Giljohann, T. C. Shad, A. K. R. Lytton-Jean, H. Min Su, and C. A. Mirkin, Science **312**, 1027 (2006).
15. H. Ju, R. A. Roy, and T. W. Murray, Biomed. Opt. Express **4**, 66 (2013).
16. X. Wang, N. Zhao, H. Liu, R. Tang, Y. Zhu, J. Xue, Z. Luo, A. Luo, and W. Xu, Chin. Opt. Lett. **13**, 81401 (2015).
17. G. Baffou, J. Polleux, H. Rigneault, and S. Monneret, J. Phys. Chem. C **118**, 4890 (2014).
18. J. R. Adleman, D. A. Boyd, D. G. Goodwin, and D. Psaltis, Nano Lett. **9**, 4417 (2009).
19. D. Huehn, A. Govorov, P. R. Gil, and W. J. Parak, Adv. Funct. Mater. **22**, 294 (2012).
20. Y. J. Zheng, Y. Wang, H. Liu, C. Zhu, S. M. Wang, J. X. Cao, and S. N. Zhu, AIP Adv. **2**, 022155 (2012).
21. N. Oara, A. S. Urban, D. Jared, L. Surbhi, N. Peter, and N. J. Halas, ACS Nano **7**, 42 (2012).
22. C. Zhao, Y. Liu, Y. Zhao, N. Fang, and T. J. Huang, Nat. Commun. **4**, 2305 (2013).
23. J. Lombard, T. Biben, and S. Merabia, Phys. Rev. Lett. **112**, 105701 (2014).
24. L. Hou, M. Yorulmaz, N. R. Verhart, and M. Orrit, New J. Phys. **17**, 1 (2014).
25. X. Liu, L. Bao, D. Michele, D. A. Francesco, and X. Zhang, Sci. Rep. **5**, 18515 (2015).